京都大学防災研究所年報 第 53 号 B 平成 22 年 6 月
Annuals of Disas. Prev. Res. Inst., Kyoto Univ., No. 53 B, 2010

Inundation Flow considering Overflow due to Water Level Rise by River Structures

Dongkeun LEE*, Hajime NAKAGAWA, Kenji KAWAIKE,
Yasuyuki BABA and Hao ZHANG

*Graduate School of Engineering, Kyoto University

Synopsis

River structures such as bridges and spur dykes cause water level rise during flood situations. Flood analysis considering this effect is very important for an accurate prediction of inundation flow. In this study, a numerical model is proposed and applied to a river channel with river structures and a river channel connected with floodplain. The numerical model is carried out on the unstructured meshes with finite volume method. The standard k-ε turbulence model and the volume of fluid (VOF) method are adopted for the turbulence closure and the free-surface modeling, respectively. The numerical simulations are carried out about the river channel with structures and the river connected with a floodplain. The proposed model is compared with the results of the experiment and another simulation. The results show tendencies of the overflow from the river and effects by the river structures with reasonable accuracy.

Keywords: inundation flow, flood analysis, river channel, floodplain, river structures

1. Introduction

Flood disasters caused by typhoon and heavy rainfall are frequently occurring all over the world. In urban area, the flood disasters divided into the river water flooding like levee overtopping and the inundation due to insufficient drainage capacity of the sewer. In the former case, the estimation of overflow discharge from the river channel is very important for the reduction of the flood damages. Many inundation analysis models have been suggested, but there are few or no models considering complicated flow within river as well. The river structures such as bridge and spur dyke generate the water level rise during a flood situation. Therefore, the consideration of the water level rise by river structures is necessary for exact prediction of flood inundation area. Three-dimensional (3D) model is required for exact prediction of the overflow discharge by river structures because two-dimensional (2D) model is not sufficient to estimate the flows around river structures. In this study, in order to analyze the river water flooding exactly, the proposed numerical model is evaluated through the simulations of the overflow from a river and the water level rise by river structures.

The simulation of the flow around river structures is related to the flow with the free surface. Most of the numerical simulation of open channel flow has usually replaced the free surface with a rigid lid. This approximation is reasonable if the free water surface is simple. This approximation will generate nonphysical errors for rapidly changing free surface. There are many computing methods available to simulate the free surface. One of the most successful methods is volume of fluid (VOF) method proposed by Hirt and Nichols (1981). This method has great advantages like convenience of operation, computational accuracy and efficiency. The VOF method is a powerful approach, but it is

not known to have been implemented on the unstructured meshes. Several researchers have been used to compute the free surface on the structured meshes. However, instances of non-physical deformation of the free surface shape also have been reported (Ashgriz and Poo, 1991; Lafauie et al., 1994; Ubbink, 1997). Therefore, in this paper, a differencing scheme proposed by Ubbink and Issa (1999) is used to improve the computation of the free surface. The proposed methodology is applied to two cases of a river connected with a floodplain and a river with river structures.

2. Numerical model

In this study, 3D Reynolds-Averaged Navier-Stokes (RANS) model proposed by Zhang et al. (2005) is employed and improved to simulate the free-surface flow. The model is carried out on the unstructured meshes with finite volume procedure. The proposed model is applied to estimate the flows considering the overflow from the river channel without structures and the water level rise in the river channel with structures. The results of the former case are compared with the results by 2D horizontal (2DH) model proposed by Zhang et al. (2006) and the latter case is compared with the experimental results.

2.1 Governing equations

3D modeling in engineering practice is built upon the RANS equations with the turbulence closure method. 2DH model can be used with advantage in case of the mean flow quantities varying but little in the vertical direction. The governing equation is obtained by integrating those in 3D model from the riverbed to the free-surface.

(1) 3D RANS model

The governing equations for continuity and momentum with the tensor notation are as follows:

$$\frac{\partial u_i}{\partial x_i} = 0 \tag{1}$$

$$\frac{\partial u_i}{\partial t} + u_j \frac{\partial u_i}{\partial x_j} = g_i - \frac{1}{\rho}\frac{\partial p}{\partial x_i} + \nu \frac{\partial^2 u_i}{\partial x_j \partial x_j} + \frac{1}{\rho}\frac{\partial \tau_{ij}}{\partial x_j} \tag{2}$$

where t is the time; u_i is the time-averaged velocity; x_i is the Cartesian coordinate component; ρ is density of the fluid; g_i is body force; p is the time-averaged pressure; ν is molecular kinematic viscosity; τ_{ij} are the Reynolds stress tensors; α is volume fraction function. The standard k - ε model is used for the turbulent flow field. The Reynolds stress tensors are acquired through the linear constitutive equation:

$$\tau_{ij} = -\overline{u_i u_j} = 2\nu_t S_{ij} - \frac{2}{3}k\delta_{ij} \tag{3}$$

where k is the turbulent kinetic energy; δ_{ij} is the Kronecker delta; ν_t is the eddy viscosity and S_{ij} is the strain rate tensor defined as:

$$\delta_{ij} = \begin{cases} 1 & if \quad i = j \\ 0 & if \quad i \neq j \end{cases} \tag{4}$$

$$\nu_t = C_\mu \frac{k^2}{\varepsilon} \tag{5}$$

$$S_{ij} = \frac{1}{2}\left(\frac{\partial u_i}{\partial x_j} + \frac{\partial u_j}{\partial x_i}\right) \tag{6}$$

where ε is dissipation rate of turbulence kinetic energy. The two transport equations are employed to estimate k and ε:

$$\frac{\partial k}{\partial t} + u_j \frac{\partial k}{\partial x_j} = \frac{\partial}{\partial x_j}\left[\left(\nu + \frac{\nu_t}{\sigma_k}\right)\frac{\partial k}{\partial x_j}\right] + G - \varepsilon \tag{7}$$

$$\frac{\partial \varepsilon}{\partial t} + u_j \frac{\partial \varepsilon}{\partial x_j} = \frac{\partial}{\partial x_j}\left[\left(\nu + \frac{\nu_t}{\sigma_\varepsilon}\right)\frac{\partial \varepsilon}{\partial x_j}\right] + (C_{1\varepsilon}G - C_{2\varepsilon}\varepsilon)\frac{\varepsilon}{k} \tag{8}$$

where G is the production rate of the turbulent kinetic energy k and is defined as:

$$G = -\overline{u_i' u_j'}\frac{\partial u_i}{\partial x_j} \tag{9}$$

The constants in equations (5), (7) and (8) take the values suggested by Rodi (1980) and generally the universal values are as follows:

$$C_\mu = 0.09 \quad C_{1\varepsilon} = 1.44 \quad C_{2\varepsilon} = 1.92$$

$$\sigma_k = 1.00 \quad \sigma_\varepsilon = 1.30 \tag{10}$$

(2) 2DH model

Integrating the governing equations in 3D model from the riverbed to the free-surface, one obtains the following equations:

$$\frac{\partial H}{\partial t} + \frac{\partial hu}{\partial x} + \frac{\partial hv}{\partial y} = 0 \tag{11}$$

$$\frac{\partial u}{\partial t} + u\frac{\partial u}{\partial x} + v\frac{\partial v}{\partial y} = -g\frac{\partial H}{\partial x} + \frac{1}{\rho h}\left[\frac{\partial h\tau_{xx}}{\partial x} + \frac{\partial h\tau_{xy}}{\partial y}\right] - \frac{\tau_{bx}}{\rho h} + D_{xx} + D_{xy} \tag{12}$$

$$\frac{\partial v}{\partial t} + u\frac{\partial v}{\partial x} + v\frac{\partial v}{\partial y} = -g\frac{\partial H}{\partial y} + \frac{1}{\rho h}\left[\frac{\partial h\tau_{yx}}{\partial x} + \frac{\partial h\tau_{yy}}{\partial y}\right] - \frac{\tau_{by}}{\rho h} + D_{yx} + D_{yy} \tag{13}$$

where H is water stage (i.e. $H=h+z_b$); h is water depth; z_b is bed elevation; x and y are Cartesian coordinate components; u and v are depth-averaged flow velocity components in the x and y directions, respectively; τ_{xx}, τ_{xy}, τ_{yx} and τ_{yy} are depth-averaged turbulent stresses; τ_{bx} and τ_{by} are bottom shear stresses; D_{xx}, D_{xy}, D_{yx} and D_{yy} are dispersion terms due to vertical non-uniformities of the mean flow. The turbulent stresses are related to the depth-averaged eddy viscosity. The two quantities k and ε are solved from their transport equations as follows:

$$\frac{\partial k}{\partial t} + u\frac{\partial k}{\partial x} + v\frac{\partial k}{\partial y} = \frac{\partial}{\partial x}\left(\frac{\nu_t}{\sigma_k}\frac{\partial k}{\partial x}\right) + \frac{\partial}{\partial y}\left(\frac{\nu_t}{\sigma_k}\frac{\partial k}{\partial y}\right) + P_h + P_{kv} - \varepsilon \tag{14}$$

$$\frac{\partial \varepsilon}{\partial t} + u\frac{\partial \varepsilon}{\partial x} + v\frac{\partial \varepsilon}{\partial y} = \frac{\partial}{\partial x}\left(\frac{\nu_t}{\sigma_\varepsilon}\frac{\partial \varepsilon}{\partial x}\right) + \frac{\partial}{\partial y}\left(\frac{\nu_t}{\sigma_\varepsilon}\frac{\partial \varepsilon}{\partial y}\right) + C_{1\varepsilon}\frac{\varepsilon}{k}P_h + P_{\varepsilon v} - C_{2\varepsilon}\frac{\varepsilon^2}{k} \tag{15}$$

where

$$P_h = \nu_t\left[2\left(\frac{\partial u}{\partial x}\right)^2 + 2\left(\frac{\partial v}{\partial y}\right)^2 + \left(\frac{\partial u}{\partial y} + \frac{\partial v}{\partial x}\right)^2\right] \tag{16}$$

$$P_{kv} = \frac{u_*^3}{hC_f^{1/2}} \tag{17}$$

$$P_{\varepsilon v} = \frac{C_{2\varepsilon}C_\mu^{1/2}}{(e_*\sigma_t)^{1/2}C_f^{3/4}}\frac{u_*^4}{h^2} \tag{18}$$

in which σ_t is Schmidt number expressing the relation between the eddy viscosity and the diffusivity for scalar transport (σ_t=1.0); e_* is dimensionless diffusivity coefficient.

2.2 Free-surface modeling

In the 3D simulation, the conservative form of the scalar convection equation for the free-surface modeling with the tensor notation as follows:

$$\frac{\partial \alpha}{\partial t} + \frac{\partial \alpha u_i}{\partial x_i} = 0 \tag{19}$$

where α is volume fraction function. The density and dynamic viscosity in the equations of motion are computed with the constitutive relations as follows:

$$\rho = \alpha\rho_1 + (1-\alpha)\rho_2 \tag{20}$$

$$\mu = \alpha\mu_1 + (1-\alpha)\mu_2 \tag{21}$$

where the subscripts 1 and 2 stand for the different fluids. The volume fraction function α is defined as follows:

$$\alpha(x,t) = \begin{cases} 1 \\ 0 \\ 0 < \alpha_\delta < 1 \end{cases} \tag{22}$$

where δ is small finite thickness. The values of α are associated with each fluid and is defined as 1 for the point (x,t) inside fluid 1, 0 for the point (x,t) inside fluid 2 and 0<α<1 for the point (x,t) inside the transitional area.

(1) Advection algorithm

The discretised transport equation for the volume fraction function α is obtained by

discretising eq. (19) as follows:

$$\alpha_P^{t+\Delta t} = \alpha_P^t + \frac{\Delta t}{V_P}\sum_f \alpha_f^* F_f \tag{23}$$

where F_f is the volumetric flux at the face. α_f^* is the approximation of the time-averaged volume fraction value at the face.

In order to calculate eq. (23) precisely, the advection algorithm to minimize the numerical diffusion of α_f^* at the face is needed. In other words, a numerical scheme to calculate α_f^* is obtained by appropriate interpolation of the value of the cell center so that maintain the boundary side of sharp gradient with the boundedness of the value. In general, the scheme is combined form of upwind differencing with and downwind differencing. The former scheme guarantees the boundedness of the value, but has large numerical diffusion. The latter is not guaranteed the boundedness of the value, but has a characteristic to conserve the boundary side with sharp gradient. The donor-acceptor scheme used generally in VOF method is using this combined form to calculate α_f^* effectively. But, this scheme has defect that shape of free-surface is deformed. Therefore, a numerical scheme is needed to avoid the numerical diffusion and non-physical deformation of the interface shape on unstructured meshes.

(2) CICSAM differencing scheme

The scheme proposed by Ubbink and Issa (1999) is employed to simulate the free-surface. The whole domain is treated as a mixture of water and air. The volume fraction is used to get the mixture properties such as density and viscosity. Most of the methods applied in volume fraction convection employ the fractional steps or operator-splitting method. Ubbink and Issa (1999) proposed CICSAM (Compressive Interface Capturing Scheme for Arbitrary Meshes) method, in which through semi implicit disposal the convection equation of the volume fraction can be solved. Particularly, this method is efficient even with unstructured meshes. The concept of normalized variable diagram and the main idea of Hirt and Nichols (1981) are employed to select diffusive scheme or dispersion scheme according to the direction of interface in this method. And, a switch parameter between diffusive and dispersion scheme is introduced to improve the accuracy of diffusive and dispersion scheme. The volume fraction at a face can be written as:

$$\alpha_f^* = (1-\beta_f)\frac{\alpha_D^t + \alpha_D^{t+\delta t}}{2} + \beta_f \frac{\alpha_A^t + \alpha_A^{t+\delta t}}{2} \tag{24}$$

where α_D is volume fraction value in donor cell; α_A is volume fraction value in acceptor cell; β_f is weighting factor.

All boundary criteria are not always satisfied even if eq. (24) is applied. According to a case, α can appear smaller than 0 or larger than 1. To revise such values, the donor-acceptor scheme used in VOF method solved by replacing non-physical values compulsorily as 0 and 1. But, revising non-physical values affect the equation of motion and cause the error of conservation quantities. In CICSAM differencing scheme, it is solved by calculating α due to predictor and corrector solution procedure. The predictor solution procedure consists of calculation of the weighting factor and volume fraction values. In order to decrease the effort of the calculation, the corrector solution procedure is executed when computational results have non-physical values.

2.3 Discretisation method

The finite volume method based on the unstructured mesh is employed and the governing equations are integrated over a number of polyhedral control volumes covering the whole domain in the finite volume method, the general form is as follows:

$$\frac{\partial}{\partial t}\int_V \varphi dV + \int_S \varphi u \cdot n dS = \int_S \Gamma \nabla\varphi \cdot n dS + \int_V b dV \tag{25}$$

where V is the volume of the control volume; S is the surface of the control volume with a unit normal vector n directing outwards; φ is the general conserved quantity representing either scalars or vector and tensor field components; Γ is the

diffusion coefficient and b is the volumetric source of the quantity φ.

The equation system is mesh independent and is valid for arbitrary polyhedral control volumes. The conserved equations are discretised on a collocated unstructured mesh. The surface fluxes are calculated from the Rhie-Chow (1983) interpolation to avoid the checkerboard variable distribution, which has caused the slow acceptance of the use of collocated mesh. The second order implicit Crank-Nicolson scheme is employed in the temporal integral. The continuity equation does not include the pressure information explicitly, but provides constraints for the velocity field. The widely used SIMPLE (Semi-implicit method for pressure-linked equations) algorithm is used for the coupling of the pressure and the velocity.

2.4 Solution methods

The final algebraic equation system resulted from the discretisation process for the iteration step n may be written as follows:

$$a_P \phi_P^n = \sum_{nb} a_{nb} \phi_P^n + b_P \tag{26}$$

Krylov subspace iterative methods considering the sparseness and non-symmetry characteristics of the coefficient matrices are preferred in this study. The iterative solver works with a suitable preconditioner. Two solvers are integrated in this study: a Bi-CGSTAB (Bi-conjugate gradient stabilized method) solver and a preconditioned GMRES (Generalized minimal residual method) solver together with an ILUTP (Incomplete LU factorization with threshold and pivoting) preconditioner (van der Vorst, 1992; Sleijpen and Fokkema, 1993; Saad, 2003).

2.5 Boundary conditions

The boundary conditions include the inlet, the outlet, and the impermeable wall.

For the inlet boundary, it is generally considered as a Dirichlet boundary and all the quantities have to be prescribed. The turbulence quantities such as k and ε are also set as constant and Neumann boundary with zero gradients is applied to the pressure. At the outlet, Neumann boundary with zero gradients can be assumed.

Near the impermeable wall, the flow velocity is assumed to be parallel to the wall. The standard wall function approach is used to link the turbulent domain with the near-wall area. The turbulence kinetic energy k and the dissipation rate ε are specified corresponding to a viscosity ratio and taking the turbulence intensity 8%. In order to represent the computational domain accurately, the unstructured meshes consist of hexahedra and quadrilateral.

3. Flood analysis of river connected with floodplain

The numerical simulations are carried out to represent the flow in a river connected with floodplain without river structures on 2D and 3D mesh, respectively. The 3D numerical results are compared with 2D numerical results and estimate the water level and the velocity.

3.1 Computational domain and conditions

The computational domain consists of a river channel and floodplains. The width of the river channel is 40cm, the width of the floodplain is 10cm and the height of the floodplain is 4cm. The initial water depth of river channel is 3cm and initial inflow discharge is $0.002 m^3/s$. The total number of mesh is 6000 quadrilateral in 2D model and 36000 hexahedra in 3D model. The discharge hydrograph expecting the overflow into the floodplain is considered by increasing the inflow discharge linearly from the initial inflow discharge and is used as inlet boundary condition. Fig. 1 and Fig. 2 show the inflow discharge hydrograph and the computational domain, respectively.

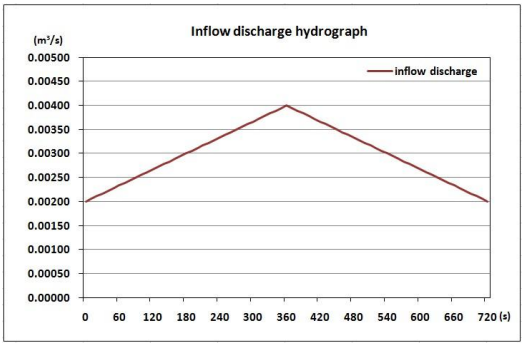

Fig. 1 Inflow discharge hydrograph

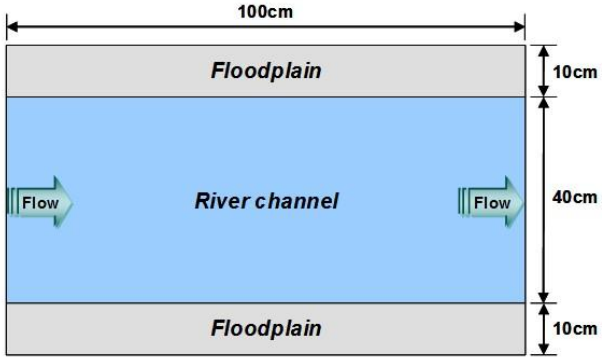

Fig. 2 Computational domain

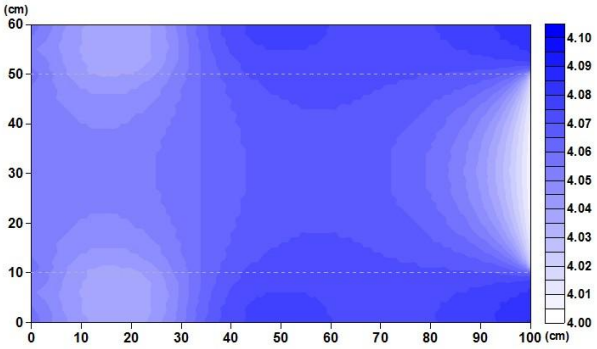

Fig. 5 Result of water level (2D model)

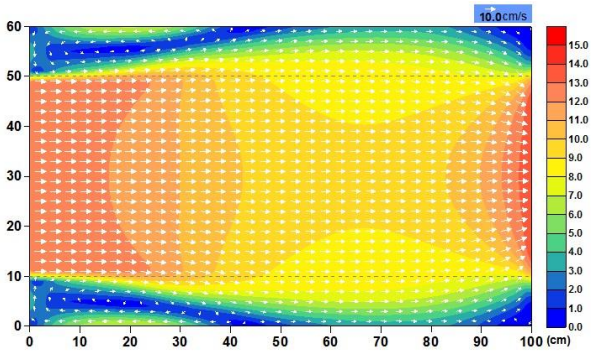

Fig. 3 Result of velocity (2D model)

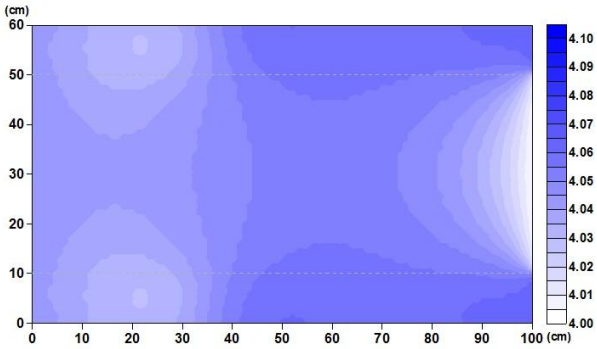

Fig. 6 Result of water level (3D model)

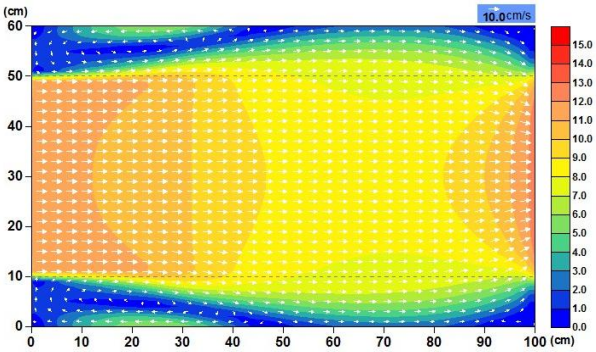

Fig. 4 Result of velocity (3D model)

3.2 Computational results

The results of the water level and the velocity obtained in the 2D and the 3D simulations are compared in this section. Figs. 3-6 are the computational results when water level overflowed from river by the increase of the inflow discharge. Fig. 3 and 4 show the results of the velocity in 2D and 3D model, respectively. Fig. 5 and 6 show the results of the water level in 2D and 3D model, respectively. In the 3D numerical simulation, the result of velocity shows by depth-averaged velocity to compare with the 2D result.

From the computational results, it is shown that the results of the velocity and water level in the 2D are slightly larger than those of the 3D, but it is judged that the results of the 2D and the 3D model have generally good agreements.

4. Flood analysis of river with structures

In the situation without considering river structures, 2D model is useful, but otherwise 2D model is not sufficient. Since 2D model is difficult to reproduce exactly the flows around river structures such as bridge pier and girder, the consideration of 3D model is necessary. In this chapter, the proposed 3D model is evaluated whether it has the reasonable accuracy for reproduction of the water level rise by the effects of river structures.

4.1 Laboratory experiments

The objective of the laboratory experiment is to compare the variations of flow according to a kind of river structures under the same hydraulic conditions. And, the laboratory experiment is

performed to compare with the numerical results.

The experimental channel used in this study is located at Ujigawa Open Laboratory, DPRI, Kyoto University and is straight channel of width 40cm, depth 23cm, and length 14.6m. The detail of the experimental conditions is described in Table 1. The experimental cases are shown in Table 2.

Case-1, Case-2 and Case-3 are the experiments to consider the effect of water level rise by the pier, girder and bridge, respectively. In the laboratory experiments, the distributions of velocity are measured at the free water surface and the depth z=2cm measured from the bottom. And, the water level is also measured for the shape of free water surface. The water gauge of servo type is used for the measurement of the shape of free water surface. The distribution of velocity at the depth z=2cm measured by using the electromagnetic velocity meter. The velocity of free water surface measured by using the PIV (Particle Image Velocimetry) method (Fujita et al., 1998). The PIV measurement is a method to determine the velocity by demanding a mean transferring distance of tracer for each measuring point based on a similarity of tracer shape between continuous pictures on the inspection domain. The PVC (Polyvinyl Chloride) powder of mean diameter 50μm is used as tracer in these experiments. The measuring domain is the range of each 50cm in the upstream and downstream side from the center of river structures. The spatial interval of measurement is 2cm.

Table 1 Hydraulic conditions (uniform flow)

Parameters	Symbols(unit)	Values
Flow discharge	$Q(l/s)$	7.00
Water depth	$h_0(cm)$	4.76
Slope	I	1/987
Mean velocity	$u_m(cm/s)$	36.80
Reynolds number	Re	17,517
Froude number	Fr	0.54

Table 2 Experimental cases

	Structures	Figure
Case-1	Cylinder pier	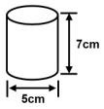
Case-2	Girder	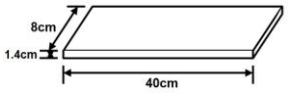
Case-3	Cylinder pier + Girder	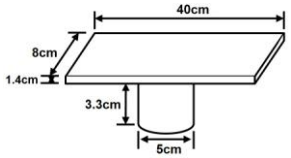

4.2 Computational results

The simulated results are compared with the experimental data. The computational domain is shown in Fig 7. The domain for comparison of the water level and the velocity at z=2cm is the range of each 150cm in the upstream and the downstream side from the center of the river structures. And, the domain for comparison of the velocity at the free water surface is the range of each 50cm in the upstream and the downstream side from center of the river structure.

(1) Results of water level

The results of plane distribution of the water level are compared in this section. Fig. 8, Fig. 9 and Fig. 10 show the results of Case-1, Case-2 and Case-3, respectively. Case-1 is not considering the overtopping flow over the river structures. Case-2 and Case-3 is considering the overtopping flow over the river structures.

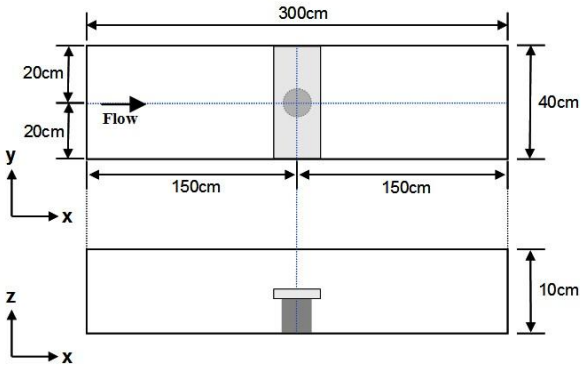

Fig. 7 Computational domains

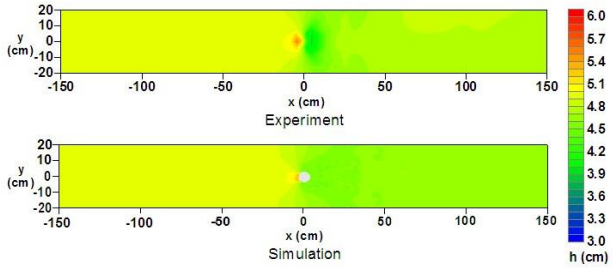

Fig. 8 Results of water level (Case-1)

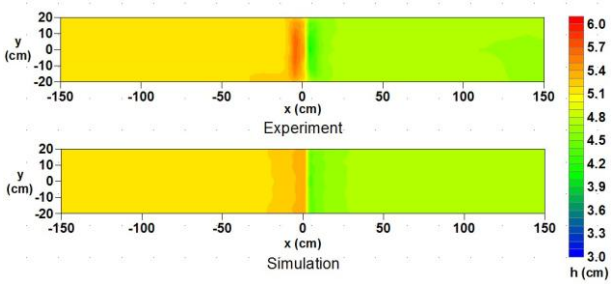

Fig. 9 Results of water level (Case-2)

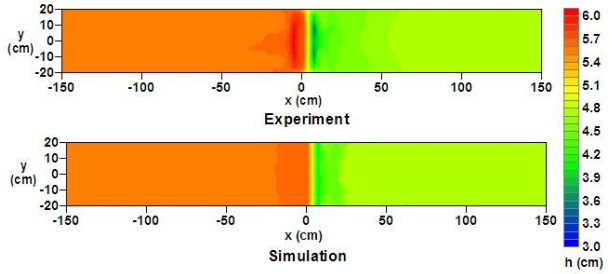

Fig. 10 Results of water level (Case-3)

In Figs. 8-10, the upper one is experimental results and the lower one is computational results. From the computational results, it is judged that the effect of backwater and water level rise by the river structures generally have good agreements although the computational results underestimate the results of water level a little than the experimental results. And, it is shown that the occupied area of the river structures in a river affects the water level rise. It is found that tendency of the water level profile can be expressed around the river structures.

(2) Comparison of water level

The water levels along the center line of the flume (y=0) in each case are shown in Figs. 11-13, respectively. The computational results of the water level are also compared with the experimental results.

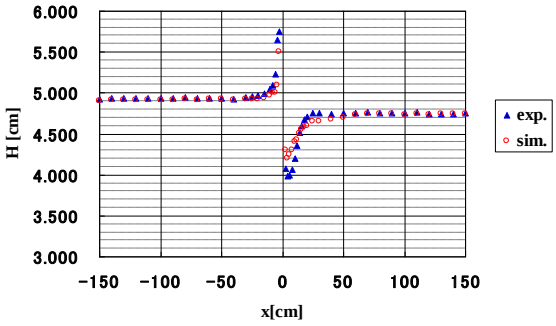

Fig. 11 Results of water level (Case-1, y=0)

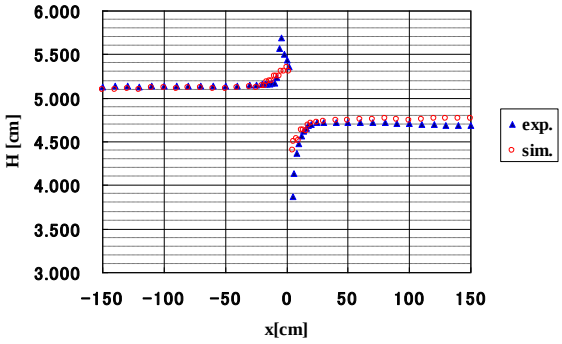

Fig. 12 Results of water level (Case-2, y=0)

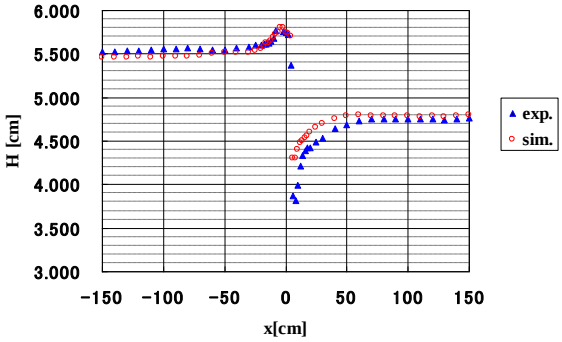

Fig. 13 Results of water level (Case-3, y=0)

In Figs. 11-13, the blue triangle is the experimental results and the red circle is the computational results. From the obtained results, it is found that the computational results of the water levels generally have good agreements with the experimental results. And, it is judged that the effect of the backwater and the water level rise by the river structures is well represented in the numerical simulations.

(3) Comparison of velocity

The computational results of the velocity at z=2cm from the bottom are compared with the experimental results as shown in Figs. 14-16.

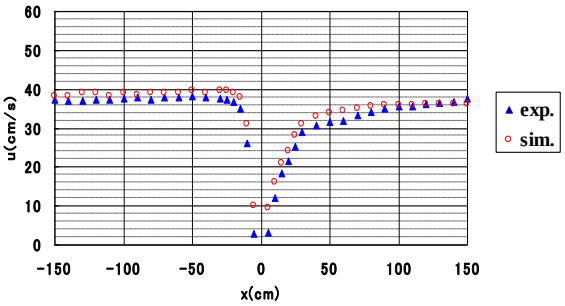

Fig. 14 Results of velocity at z=2cm (Case-1, y=0)

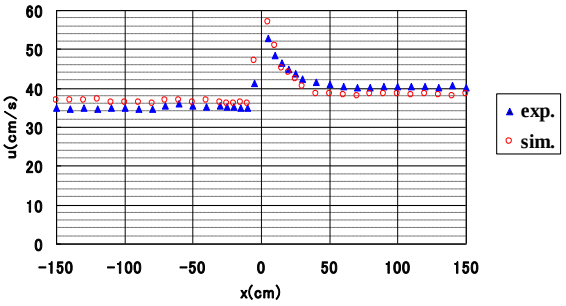

Fig. 15 Results of velocity at z=2cm (Case-2, y=0)

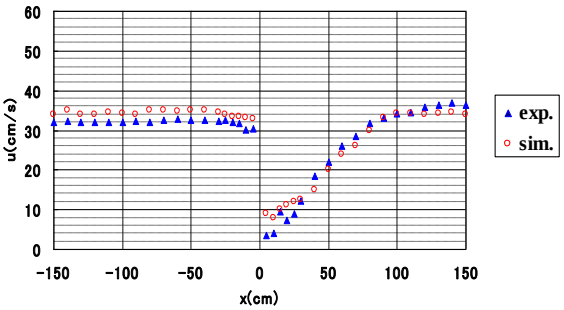

Fig.16 Results of velocity at z=2cm (Case-3, y=0)

From the above mentioned numerical results, the velocities generally have good agreements with the experimental results. In the numerical results considering river structures, the variations of velocity around the river structures could be seen.

In view of the results so far achieved, it is found that all the results generally can reproduce well the effect of the river structures, but the numerical model slightly underestimates the water level. The main causes of those under-predictions seem to be in the modeling of the turbulence. The turbulence model employed in this study is the standard k - ε model, which has several problems as pointed out by Speziale (1991), for example the inability to properly account for the streamline curvature, rotational strains and other body force effects and the neglect of the non-local and the effects of the Reynolds stress anisotropies. In order to correct these problems, the consideration of model by introducing non-linear constitutive relation between the mean strain rate and the turbulence stresses is required.

5. Conclusions

In this study, the numerical simulation was conducted to estimate the flow of a river connected with a floodplain and the effects of water level rise by the structures within a river. The proposed numerical models were treated on an unstructured mesh with finite volume method. The standard k - ε model was used for turbulence model and the volume of fluid method proposed by Hirt and Nichols (1981) was used to represent the free water surface. The differencing scheme proposed by Ubbink and Issa (1999) is also employed to compute the free water surface in unstructured mesh.

The prediction of the overflow by the river structures is very important from the viewpoint of flood disaster. The present study shows that the numerical model used in this study can be used to simulate the changes of the flow field on the river connected with floodplain and the river with structures although the results of the numerical model with the river structures underestimate the water level rise around the river structures. In order to improve the model proposed in this study, further researches considering different turbulence models, laboratory experiments and various flow conditions are necessary.

References

Ashgriz, N. and Poo, J. Y. (1991): Flux line segment model for advection and interface reconstruction, Journal of Computational Physics, Vol.39, pp.449-468.

Fujita I., Muste M., and Kruger A. (1998): Large-scale particle image velocimetry for flow analysis in hydraulic engineering applications, Journal of Hydraulic Research, Vol. 36, No. 3, pp.

397–414.
Hirt, C. W. and Nichols, B. D. (1981): Volume of fluid (VOF) method for dynamics of free boundaries, Journal of Computational Physics, Vol.39, pp.201-225.
Lafauie, B., Nardone, C., Scardovelli, R., Zaleski, S. and Zanetti, G. (1994): Modelling merging and fragmentation in multiphase flows with SURFER, Journal of Computational Physics, Vol.113, pp.134-147.
Rhie, C. M. and Chow, W. L. (1983): A numerical study of the turbulent flow past an isolated airfoil with trailing edge separation, AIAA Journal, Vol.21, pp.1525-1532.
Rodi, W. (1980): Turbulence models and their application in hydraulics-a state of the art review, University of Karlsruhe, Karlsruhe, Germany.
Saad, Y. (2003): Iterative methods for sparse linear system (second edition), Society for Industrial & Applied Mathematics.
Sleijpen, G. L. G. and Fokkema, D. R. (1993): BiCGSTAB (l) for linear equations involving unsymmetrical matrices with complex spectrum, Electronic Transactions on Numerical Analysis, Kent State University, Vol.1, pp.11-32.
Speziale C. G. (1991): Analytical methods for the development of Reynolds-stress closures in turbulence, Annual Review of Fluid Mechanics, Vol. 23, pp. 107–157.
Ubbink, O. (1997): Numerical prediction of two fluid systems with sharp interfaces, Ph.D. thesis, University of London.
Ubbink, O. and Issa, R. I. (1999): A method for capturing sharp fluid interfaces on arbitrary meshes, Journal of Computational Physics, Vol.153, pp.26-50.
van der Vorst, H. A. (1992): Bi-CGSTAB: a fast and smoothly converging variant of Bi-CG for the solution of non-symmetrical linear systems, SIAM Journal on Scientific and Statistical Computing, Vol.13(2), pp.631-644.
Zhang, H., Nakagawa, H., Ishigaki, T., Muto, Y. (2005): A RANS solver using a 3D unstructured FVM procedure, Annuals of Disaster Prevention Research Institute, Kyoto University, No.48 B.
Zhang, H., Nakagawa, H., Muto, Y., Touchi, D. and Muramoto, Y. (2006): 2D numerical model for river flow and bed deformation based on unstructured mesh, Journal of Applied Mechanics, JSCE, Vol.9, pp. 783-794.

河川構造物による水位上昇を考慮した氾濫流

Dongkeun LEE*・中川一・川池健司・馬場康之・張浩

*京都大学大学院工学研究科

要　旨

橋や水制のような河川構造物は洪水時に水位上昇の原因となり，この影響を考慮した洪水解析は氾濫流の正確な予測のために重要である。本研究では，このような流れ場を計算するための数値モデルを提案し，河川構造物を有する河川水路および河川水路と氾濫原が一体となった領域に適用する。この数値モデルでは非構造格子を用いた有限体積法によって計算を実行しており，乱流モデルには標準$k-\varepsilon$モデルを，自由水面のモデル化にはVOF法を用いている。提案された数値モデルは実験結果や既往の数値モデルの解析結果と比較し，検討を行った。その結果，河川構造物の影響と河川水路からの氾濫流の傾向を，妥当な精度を持って表現できることを確認した。

キーワード：氾濫流，洪水解析，河川水路，氾濫原，河川構造物